Influence of Heat Treatment on Corrosion Resistance of Sn/Mg Films Formed by PVD Method on Hot-Dip Galvanized Steel

Sung-Hwa Hwang [1] , **Seung-Hyo Lee [2]** **and Myeong-Hoon Lee [1,3,*]**

1 Department of Marine Engineering, Korea Maritime and Ocean University, Busan 49112, Republic of Korea
2 Department of Ocean Advanced Materials Convergence Engineering, Korea Maritime and Ocean University, Busan 49112, Republic of Korea
3 Interdisciplinary Major of Maritime AI Convergence, Korea Maritime and Ocean University, Busan 49112, Republic of Korea
* Correspondence: leemh@kmou.ac.kr

Abstract: Double layers composed of Sn and Mg, each 0.8 μm thick, were fabricated on a hot-dip galvanized steel (8.4 μm) sheet using DC magnetron sputtering and post-annealing processes. With an increase in temperature, the surface morphologies were agglomerated with each other. Additionally, Sn/Mg mixture sites, including an intermetallic compound of Mg_2Sn, were formed at 190 °C and locally clustered at 220 °C. In the salt-spray test, the corrosion resistance of the Sn/Mg film prepared at 190 °C was 960 h, which is longer than that at non-heat for 528 h or 220 °C for 480 h. In the polarization test, the Sn/Mg film formed at 190 °C displayed a lower corrosion current density of 1.07 μA/cm^2 and potential of 1.62 V/SSCE than those at non-heat or 220 °C.

Keywords: corrosion resistance; hot-dip galvanized steel; physical vapor deposition; heat treatment; intermetallic compounds; salt spray test; potentio dynamic polarization test

1. Introduction

Hot-dip galvanized steel (HDG) has played an important role in improving the corrosion resistance of steels used in the automotive and construction industries owing to its outstanding mechanical properties and durability in corrosive environments [1–3]. Generally, increasing the Zinc coating thickness and adding metallic components, such as Al and Mg, are considered to improve the corrosion resistance of HDG, which combines the sacrificial protection of Zn based alloy and the physical barrier of Al oxide film [4–8]. However, the conventional process for HDG often entails drawbacks, including catalyst impurities and large resource consumption to maintain a molten bath [9,10]. Therefore, alternative methods have been proposed. One potential technique is thermal spray coatings using a stream of feedstocks which is dependent on the thermal expansion gradient between the top coat and the substrates [11,12]. Another promising method is physical vapor deposition (PVD) which provides various coating layers because it has few restrictions on source materials and the formation of multi-layers [13–17].

So far, several studies have been reported about the corrosion resistance of Al, Mg, and Zn films prepared by the PVD method. Jeong et al. explained that the Mg layer deposited by the PVD method prevents the penetration of oxygen species by forming Mg corrosion products at the grain boundary of the base material [10,18]. La and Park et al. showed the effectiveness of the Zn–Mg coating layer on corrosion resistance regarding the formation of protective corrosion products [19,20]. Byun et al. suggested intermetallic compounds (IMPc) such as Mg_2Zn, Al_3Mg_2, and Mg_2Si be related to the delay in fitting corrosion [10,21].

Although these PVD methods suggest an effective methodology on how to improve the corrosion resistance of steels, the approaches are limited to more active elements, Al, Zn, and Mg, than Fe. Moreover, the electro potential difference between the metals

causes the galvanic corrosion of base materials, which puts the usage of less active metals aside. Additionally, few studies have been conducted on the application of PVD and post-annealing processes.

In this study, Sn and Mg were applied as the coating layers because Sn is the least active and Mg is the most active element among the most accessible metals [22–24]. Sn/Mg thin films were prepared by the PVD method and annealed under different heating conditions. The prepared Sn/Mg films showed improved corrosion resistance depending on temperature. The findings of this study are expected to shed light on the fabrication of super anti-corrosive coatings based on the PVD process with various metals.

2. Materials and Methods

2.1. Formation of Sn/Mg Films

The Sn/Mg films were deposited using DC magnetron sputtering that includes two different coating targets, as shown in Figure 1. Both Sn and Mg targets were settled into one chamber at 60 mm to the left and 90 mm to the right from the substrate holder. The substrates (HDG steel of KS D 3506:2007, Zn thickness 8.4 μm) were attached to the rotational holder between the two targets. The substrates were cleaned away using an ultrasonic wave in ethyl alcohol and an ion-bombardment of 50 V in 3.0×10^{-1} Torr. Sn/Mg films were fabricated in three steps. Firstly, 0.8 μm-thick Mg film was deposited on the HDG substrate at a discharge power of 200 W for 20 min. Secondly, Sn film with a 0.8 μm thickness was deposited on the top of the Mg layer one after another. For both depositions, base pressure, working pressure and substrate temperature remained the same as 3×10^{-6} Torr, 3×10^{-2} Torr and 20 °C, respectively. Additionally, 100 sccm of Ar gas was introduced into the chamber for sputtering. Table 1 presents information about the prepared Sn/Mg film and other competitive samples. Lastly, the deposited Sn/Mg film was annealed at three different heating conditions: non-heat (as coated), 190 °C for 30 min, and 220 °C for 30 min in atmospheric conditions. The temperature was set at 204 °C, where the eutectic reaction takes place in the Sn–Mg binary phase diagram, to form the IMPc [21,25]. In the pilot experiment, we found the color change and the film delamination simultaneously when Sn was heat treated at over 232 °C. This is probably due to the difference in thermal stress of the local area adjacent to the Sn and Mg layers [26].
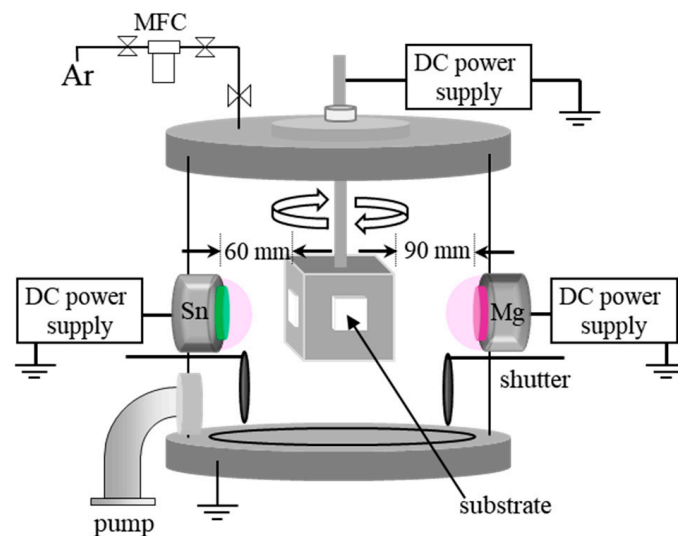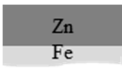

Figure 1. Schematic diagram of the DC magnetron sputtering for the fabrication of Sn/Mg film.

Table 1. Information about the samples in this study: Sn/Mg film; Mg film; Sn film; and substrate.

Samples	Schematic Diagram	Sn Thickness (μm)	Mg Thickness (μm)	Zn Thickness (μm)
Sn/Mg Film (As coated)		0.8	0.8	
Mg Film		-	1.6	8.4 (Hot-dip Galvanized Steel – KS D 3506:2007)
Sn Film		1.6	-	
HDG (Substrate)		-	-	

2.2. Methods for Film Characterization

The Sn/Mg film morphologies of the top surface and the cross-section were observed using FE-SEM (Field Emission Scanning Electron Microscope, MIRA 3, Tescan Brno, Czech Republic). To confirm the effectiveness of heat treatment in coating layers, the components, depth profile, and crystal phase were analyzed using EPMA (Electron Probe X-Ray Microanalyzer, JEOL, Tokyo, Japan), GD-OES (Glow Discharge Optical Emission Spectrometry, HORIBA, Kyoto, Japan) and XRD (High Resolution X-Ray Diffractometer, SmartLab, Rigaku, Tokyo, Japan).

To evaluate the corrosion resistance of Sn/Mg films, a salt spray test (SST) was carried out in accordance with ISO 9227 (5% NaCl solution, maintenance at 35 °C). Here, the surface of the specimen was periodically observed, and the initial occurrence of red rust was recorded. Additionally, a potentio dynamic polarization test was conducted in a 3.5% NaCl solution by potentio-stat (Interface 1000, Gamry Ins., Warminster, PA, USA). The scan rate was 1 mV/s from −0.1 V to +1.5 V, and the Pt counter electrode and the Ag/AgCl reference electrode were employed. The corrosion current density (I_{corr}) and potential (E_{corr}) were obtained by Tafel Extrapolation. Furthermore, we monitored the corrosion state of the Sn/Mg films throughout the polarization test to confirm the corrosion process. After collecting the samples, we rinsed their surfaces with pure water three times. Then we observed the film surface using SEM and EDS.

3. Results and Discussion

3.1. Morphologies, Components and Crystallinity

In general, the corrosion resistance of thin films highly depends on their morphology and chemical components [25,27]. To date, much research data dealing with the heat treatment of HDG have reported the component and the phase transition through atomic diffusion at high temperatures [28–31]. Here, we analyzed the Sn/Mg films depending on heating conditions to understand the correlation between film characteristics and corrosion resistance.

In the surface images of Figure 2a–c, the small granular-shaped particles are agglomerated together. When the heating temperature increases, the agglomerated area expands, and a relatively large clustered area is identified at 220 °C.
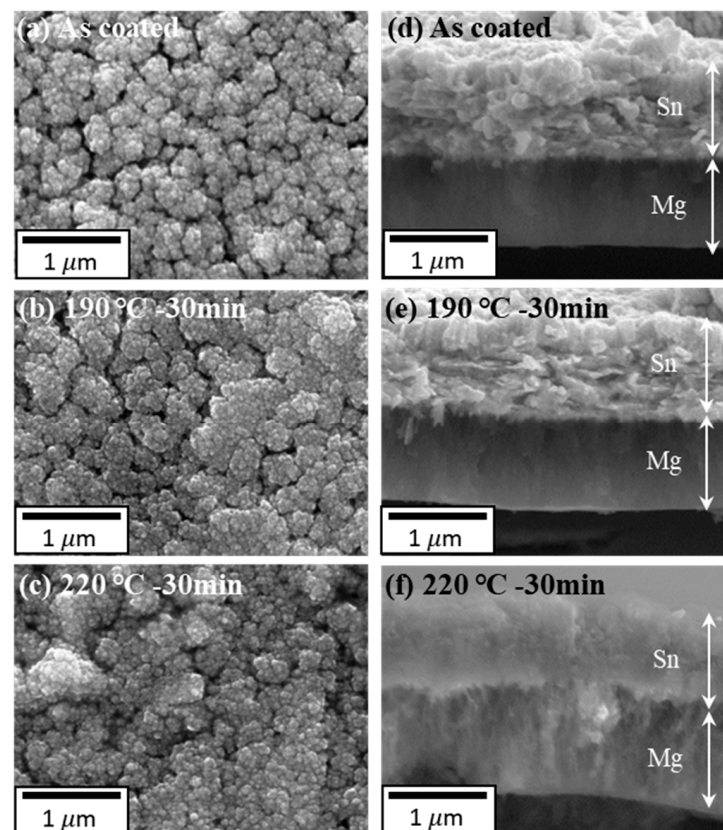
Figure 2. SEM images of Sn/Mg films as a parameter of heat treatment conditions. (**a**–**c**) Surface images. (**d**–**f**) Cross-sectional images.

As for the cross-sectional images, the Sn upper layer and the Mg under layer are clearly separated, as shown in Figure 2d,e. The thickness of the Mg and Sn coating layers was set at 0.8 μm each. The shape of the Sn layer was a granular-like structure, while the Mg layer had a featureless shape. On the other hand, in Figure 2f, the Mg layer and the interface became columnar-like structures and had indistinct shapes. Moreover, the polygon shape of the crystals that were approximately 100 nm was observed around the interface between the Sn upper and Mg lower layers.

Next, Figure 3 displays the depth profile for Sn/Mg films [32]. In Figure 3a, the Sn upper layer and the Mg lower layer are approximately 0.8 μm each in thickness and are separated. In addition, Zn has an approximately 8 um thickness, and Fe exists in the lower area. Meanwhile, in Figure 3b, the Sn layer extends down to the Mg layer area. Furthermore, the Mg layer extends up to the surface. O tends to increase gradually from the surface to the Mg layer, which indicates that O combines more easily with relatively active Mg. Subsequently, Figure 3c shows a similar trend as b, but components Zn and Fe expand more closely towards the surface. Additionally, we observed the component mapping of the Sn/Mg films in Figure 4. With an increasing heating condition, Sn tended to go down to the substrate region, while Mg and Zn went up to the surface at the same time. The Sn/Mg mixture area gradually increased, and the concentration of large amounts of Sn/Mg was verified at 220 °C, which is considered the effect of component diffusion around the interface [22,33].

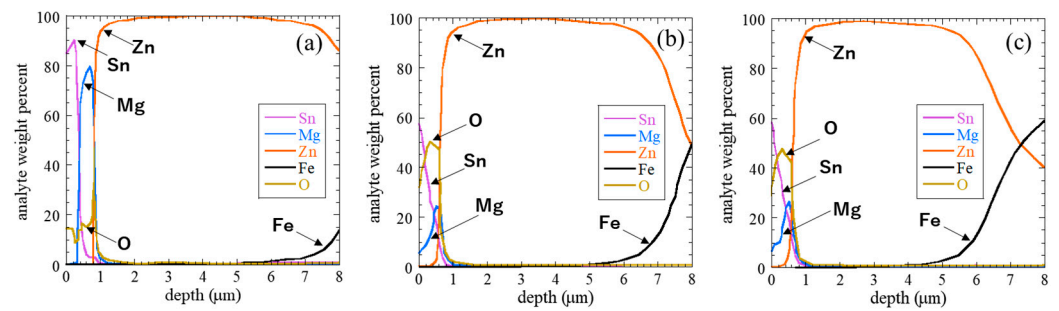**Figure 3.** GD-OES depth profile for Sn/Mg films as a parameter of heat treatment. (**a**) As coated, (**b**) 190 °C for 30 min, and (**c**) 220 °C for 30 min.
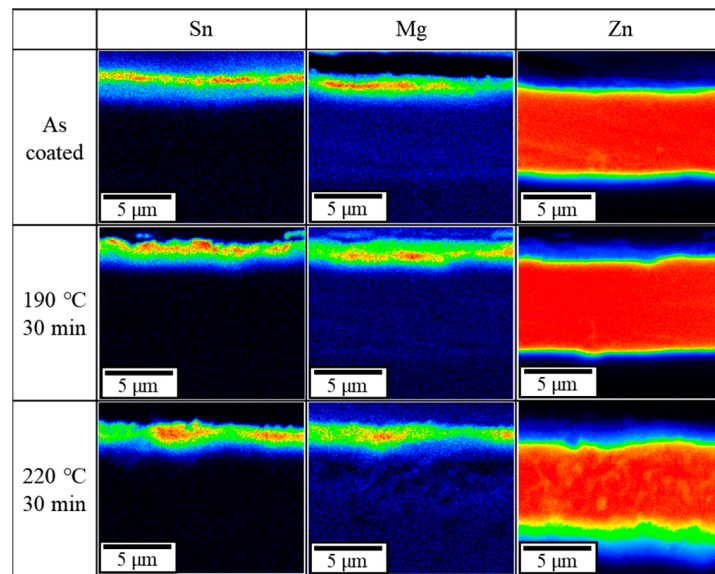

Figure 4. EPMA mapping images of Sn/Mg films as a parameter of heat treatment.

Figure 5 shows the XRD patterns of the Sn/Mg films as a parameter of heating conditions. To clearly visualize the peaks of the XRD pattern, we plotted the graph with a log scale. In Figure 5a, for an as-coated condition, Sn (30.6, 31.9, 44.7 degrees), Mg (32.6, 34.6, 36.2 degrees), and Zn (36.3, 39, 43.2 degrees) spectra are obtained, whereas the heat-treated Sn/Mg films represent not only Sn, Mg, and Zn but also the SnO (29.5, 33.2, 50.7 degrees) and Mg_2Sn (22.7, 37.3, 43.8 degrees) spectra in Figure 5b,c [34,35]. Furthermore, we compared the ratio of relative intensity (I_{Sn} 30.6; I_{Mg} 32.6; I_{Zn} 43.2; I_{SnO} 29.5; I_{Mg2Sn} 22.7) for quantitative analysis. The ratio is an alternative index related to volume fraction [36]. The I_{Sn} and I_{Zn} decrease from 9.24% and 87.3% at as coated to 9.12% and 74.8% at 190 °C, and 8.82% and 80.2% at 220 °C. The I_{Mg} increases from 3.54% at as coated to 5.92% at 190 °C and 5.61% at 22 0°C. On the other hand, I_{SnO} sharply drops from 8.57% at 190 °C to 3.52% at 220 °C. I_{Mg2Sn} barely changes from 1.83% at 190 °C to 1.87% at 220 °C. These imply that the amount of Mg_2Sn was almost constant at both 190 °C and 220 °C, but Sn moved below the interface of Sn and Mg layer and clustered with a large mass that restrained the formation of the SnO film on the top surface at 220 °C [21].
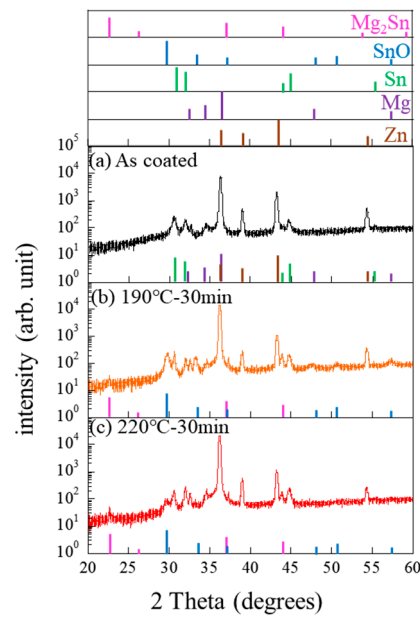
Figure 5. XRD patterns of Sn/Mg films. (**a**) As coated, (**b**) 190 °C for 30 min and (**c**) 220 °C for 30 min.

3.2. Salt Spray Test

Among various methods to evaluate the corrosion resistance of surface coatings, SST is considered a powerful tool that aims to observe not only the degree of corrosion protection to the underlying materials, but also the time evolution of the corrosion products [37,38]. Since red rust is caused by the exposure of the internal iron to an external corrosion site, resulting in its oxidation, we marked the initiation time of red rust as the end point of film protection. Figure 6 shows the digital images of SST of the Sn/Mg films and the competitive ones. The initiation time of the Sn/Mg film at 190 °C was 960 h, which is far longer than that of 528 h at non-heat (as coated) or 480 h at 220 °C. Furthermore, Sn/Mg films with a 1.6 μm thickness on HDG at 190 °C showed highly improved corrosion resistance compared to other samples, such as Sn or Mg single films with 1.6 μm thickness on HDG and even the conventional 20 μm-thick HDG.

Figure 6. SST images of Sn/Mg and other films. The red dot indicates the initiation point of red rust.

Additionally, we observed the surface covering behavior of the corrosion products. HDG is known to form white corrosion products in SST, such as $Zn_5(CO_3)_2(OH)_6$ (Hydrozincite) or $Zn_5(OH)_8Cl_2H_2O$ (Simonkolleite), which temporarily delay the degradation of the film surface by isolating the critical pitting area from the corrosion factors [39–41]. From the SST images, white corrosion products were observed in all films before the red

rust initiation. In particular, Sn/Mg films prepared at 190 °C and 220 °C showed a gradual expansion of surface covering areas with corrosion products. This is probably related to the continuous protection of the barriers and the sacrificial anodic effects on the corrosion spot.

Since Mg-containing IMPc can change its polarity during the corrosion process [24,42–44], it keeps influencing the pitting- or galvanic corrosion by supplying electrons to the films adjacent to IMPs as sacrificial anodes. In contrast, the excessive heat of 220 °C, which leads to morphology changes and the formation of localized mixing sites, rather decreases the anti-corrosive performance. Based on the above discussions, the heat treatment of an Sn/Mg film is an important key to improving corrosion resistance.

3.3. Potentiodynamic Polarization Test

The potentiodynamic polarization test is a relatively non-destructive technique to evaluate the corrosion characteristics. It provides electrochemical information, such as corrosion current density (I_{corr}), corrosion potential (E_{corr}), and passive state [45]. To understand the role of each component, firstly, we examined the HDG (substrate) and the Sn and Mg single layer on HDG, as shown in Figure 7a. A conventional HDG has an I_{corr} of 1.99 µA/cm^2 and an E_{corr} of -1.05 µV. The Sn single film has an I_{corr} of 0.84 µA/cm^2 and an E_{corr} of -1.24 µV, which are caused by the protective barrier effect of Sn oxide at the beginning of corrosion. A Mg single film has an I_{corr} of 125 µA/cm^2 and an E_{corr} of -1.68 µV. Additionally, the Mg curve represents the passivation region between -1.59 µV and -1.06 µV, where corrosion does not occur.
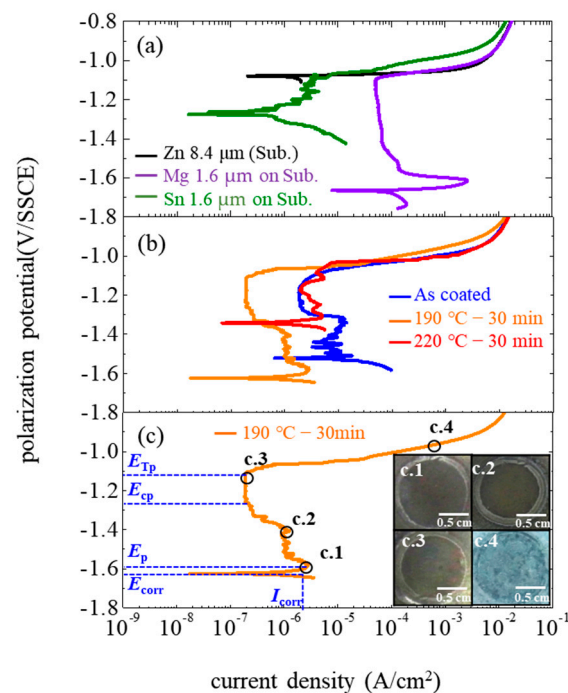

Figure 7. Polarization curves of Sn/Mg films and competitive films. (**a**) competitive films; HDG substrate; Mg and Sn single film on HDG. (**b**) Sn/Mg films depending on heating conditions. (**c**) digital images at four different points of the polarization test with Sn/Mg films prepared at 190 °C. I_{corr}−corrosion current density; E_{corr}−corrosion potential; E_p−passivation potential; E_{cp}−passivation complete potential; E_{Tp}−transpassive potential.

Figure 7b displays the polarization curve of the Sn/Mg films as a parameter of heating conditions. The non-heated Sn/Mg film has an I_{corr} of 9.11 µA/cm^2 and an E_{corr} of -1.53 µV, and the curve includes an unstable active state and a passive region. This may be attributed to the galvanic corrosion of Sn and Mg components. Next, the Sn/Mg film prepared at 190 °C has an I_{corr} of 1.07 µA/cm^2, an E_{corr} of -1.62 µV , and a passivation region between -1.58 µV and -1.08 µV. Here, I_{corr} continuously decreases from 1.23 µA/cm^2

at -1.58 µV (E_p) to 0.11 µA/cm² at 1.27 µV (E_cp). On the other hand, the Sn/Mg film prepared at 220 °C has an I_corr of 2.44 µA/cm², an E_corr of -1.36 µV, and the passive region is relatively short and unstable. Namely, the heat treatment of Sn/Mg films at 190 °C contributes to improving corrosion resistance in terms of the reduction of corrosion current density and the formation of a passivation region.

Figure 7c represents the digital images at four different points on the polarization curve of the Sn/Mg films prepared at 190 °C. We distinguished the points as (c.1) for the beginning of the passivation state, (c.2) for the middle of the passivation state, (c.3) for the beginning of the transpassive state, and (c.4) for the transpassive state. In the digital images, an almost identical circle with a corrosion area of 0.785 cm² is observed in (c.1)–(c.3), whereas the white corrosion products on the entire surface of the circle are shown in (c.4). To analyze the corrosion mechanism of the Sn/Mg film prepared at the level of 190 °C, we carried out a point analysis of Figure 7(c.1)–(c.4) using SEM and EDS as follows.

In Figure 8(c.1), partially agglomerated white precipitates exist on the film surface. The composition of the precipitates was approximately 7% of Sn, 14% of Mg, 1% of Zn and 78% of O, while the matrix was composed of about 3% of Sn, 25% of Mg, 1% of Zn and 71% of O. In Figure 8(c.2,c.3), the size of the precipitates gradually decreases regardless of the composition change, and the amount of Sn and Zn slightly increases at places without precipitates. In Figure 8(c.4), large-clustered precipitates are observed on the surface, and their composition is approximately 1% of Sn, 4% of Mg, 26% of Zn and 62% of O, whereas crevices between the large precipitates include about 8% of Sn, 9% of Mg 17% of Zn and 62% of O. EDS spectra show the typical composition of the Sn/Mg film after the polarization test and are categorized into four types (Type A–Type D) depending on the compositions. To sum up, the white precipitates contain Mg and Sn with a constant ratio, and their size decreases as passivation progresses in Figure 8(c.1–c.3). On the other hand, the large masses in Figure 8(c.4) are regarded as Zn corrosion products that formed at a transpassive state.
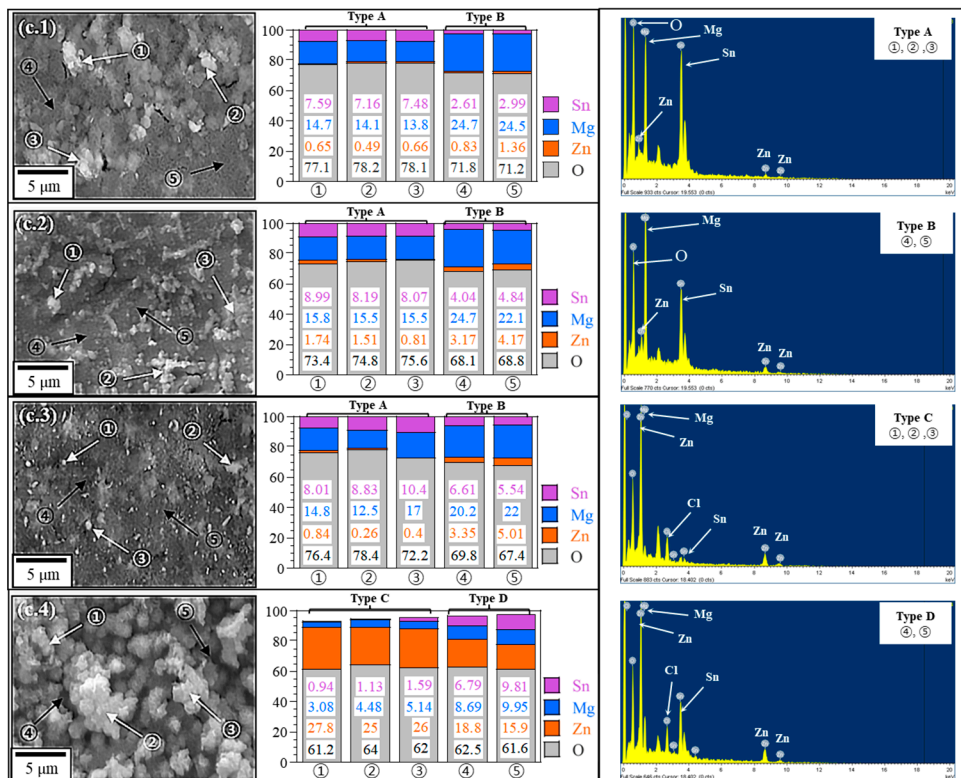

Figure 8. SEM images and EDS components at four different points in Figure 7c. The white arrows indicate the location of the white precipitates and the black arrows indicate the matrix. The bar graphs display the composition of arrows from 1 to 5 at left SEM images. The compositions are categorized to four different types from A to D in terms of SEM images and their compositions.

These results evidently imply that the Sn/Mg mixture area containing Mg$_2$Sn enhanced the corrosion resistance. Additionally, it is considered that the formation of a protectable Sn oxide film on the surface and the maintenance of the passivation state without critical galvanic corrosion with the heat treatment of 190 °C coincide with the higher corrosion resistance at SST.

4. Conclusions

We successfully fabricated Sn/Mg films on HDG through a PVD method and a post-annealing process. The corrosion resistance of Sn/Mg film was highly improved at a heating temperature of 190 °C as compared to non-heat and 220 °C. The findings of this study are as follows:

- With an increase in temperature, the surface morphology of the Sn/Mg films agglomerated with each other. The cross-sectional morphology changed from a granular- at non-heat to a columnar-like structure at 190 °C, and to an indistinct shape at 220 °C.
- Sn/Mg mixture areas, including Mg$_2$Sn, were formed at over 190 °C. Additionally, locally clustered Sn/Mg sites on the top surface were identified at 220 °C.
- In the salt spray test, the red rust initiation time of the Sn/Mg film prepared at 190 °C was 960 h, which is longer than that at non-heat for 528 h or 220 °C for 480 h.
- From the polarization test, we found that the Sn/Mg film prepared at 190 °C has a lower I_{corr} of 1.07 μA/cm^2 and E_{corr} of −1.62 μV, and an enhanced passive region in comparison with the film prepared at non-heat or 220 °C.
- The Sn/Mg mixture area including Mg$_2$Sn contains Mg and Sn in a constant ratio, and their size decreases as passivation progresses, which maintains the passivation state with stability.

Author Contributions: Formal analysis, S.-H.H.; writing—original draft preparation, S.-H.H., S.-H.L. and M.-H.L.; writing—review and editing, supervision, M.-H.L.; funding acquisition, M.-H.L. All authors have read and agreed to the published version of the manuscript.

Institutional Review Board Statement: Not applicable.

Informed Consent Statement: Not applicable.

Data Availability Statement: Data are contained within the article.

Conflicts of Interest: The authors declare no conflict of interest.

References

1. Shreyas, P.; Panda, B.; Vishwanatha, A.D. Embrittlement of Hot-Dip Galvanized Steel: A Review. *AIP Conf. Proc.* **2021**, *2317*, 1–15. [CrossRef]
2. Li, G.; Long, X. Mechanical Behavior and Damage of Zinc Coating for Hot Dip Galvanized Steel Sheet DP600. *Coatings* **2020**, *10*, 202. [CrossRef]
3. Peng, S.; Xie, S.K.; Xiao, F.; Lu, J.T. Corrosion Behavior of Spangle on a Batch Hot-Dip Galvanized Zn-0.05Al-0.2Sb Coating in 3.5 Wt.% NaCl Solution. *Corros. Sci.* **2020**, *163*, 1–8. [CrossRef]
4. Shibli, S.M.A.; Meena, B.N.; Remya, R. A Review on Recent Approaches in the Field of Hot Dip Zinc Galvanizing Process. *Surf. Coatings Technol.* **2015**, *262*, 210–215. [CrossRef]
5. de Rincón, O.; Rincón, A.; Sánchez, M.; Romero, N.; Salas, O.; Delgado, R.; López, B.; Uruchurtu, J.; Marroco, M.; Panosian, Z. Evaluating Zn, Al and Al–Zn Coatings on Carbon Steel in a Special Atmosphere. *Constr. Build. Mater.* **2009**, *23*, 1465–1471. [CrossRef]
6. Qiu, P.; Leygraf, C.; Odnevall Wallinder, I. Evolution of Corrosion Products and Metal Release from Galvalume Coatings on Steel during Short and Long-Term Atmospheric Exposures. *Mater. Chem. Phys.* **2012**, *133*, 419–428. [CrossRef]

7. Song, G.L.; Dudney, N.J.; Li, J.; Sacci, R.L.; Thomson, J.K. The Possibility of Forming a Sacrificial Anode Coating for Mg. *Corros. Sci.* **2014**, *87*, 11–14. [CrossRef]

8. Hosking, N.C.; Ström, M.A.; Shipway, P.H.; Rudd, C.D. Corrosion Resistance of Zinc-Magnesium Coated Steel. *Corros. Sci.* **2007**, *49*, 3669–3695. [CrossRef]

9. Park, J.-H.; Ko, K.-P.; Hagio, T.; Ichino, R.; Lee, M.-H. Effect of Zn-Mg Interlayer on the Corrosion Resistance of Multilayer Zn-Based Coating Fabricated by Physical Vapor Deposition Process. *Corros. Sci.* **2022**, *2022*, 110330. [CrossRef]

10. Park, G.D.; Yang, J.H.; Lee, K.H.; Kim, H.J.; Lee, S.H.; Kang, J.; Yun, Y.S.; Lee, M.H. Ultra-High Corrosion Resistance of Al-Mg-Si Film on Steel Sheet Formed by PVD Mg Coating and Heat Treatment. *Corros. Sci.* **2021**, *192*, 109829. [CrossRef]

11. Thakare, J.G.; Pandey, C.; Mahapatra, M.M.; Mulik, R.S. Thermal Barrier Coatings—A State of the Art Review. *Met. Mater. Int.* **2021**, *27*, 1947–1968. [CrossRef]

12. Thakare, J.G.; Pandey, C.; Mulik, R.S.; Mahapatra, M.M. Mechanical Property Evaluation of Carbon Nanotubes Reinforced Plasma Sprayed YSZ-Alumina Composite Coating. *Ceram. Int.* **2018**, *44*, 6980–6989. [CrossRef]

13. Lee, M.; Bae, I.; Kwak, Y.; Moon, K. Effect of Interlayer Insertion on Adhesion Properties of Zn-Mg Thin Films on Steel Substrate by PVD Method. *Curr. Appl. Phys.* **2012**, *12*, S2–S6. [CrossRef]

14. Hwang, S.H.; Okumura, T.; Kamataki, K.; Itagaki, N.; Koga, K.; Nakatani, T.; Shiratani, M. Low Stress Diamond-like Carbon Films Containing Carbon Nanoparticles Fabricated by Combining Rf Sputtering and Plasma Chemical Vapor Deposition. *Jpn. J. Appl. Phys.* **2020**, *59*, 100906. [CrossRef]

15. Dan, A.; Bijalwan, P.K.; Pathak, A.S.; Bhagat, A.N. A Review on Physical Vapor Deposition-Based Metallic Coatings on Steel as an Alternative to Conventional Galvanized Coatings. *J. Coat. Technol. Res.* **2022**, *19*, 1–36. [CrossRef]

16. Hwang, S.-H.; Iwamoto, R.; Okumura, T.; Kamataki, K.; Itagaki, N.; Koga, K.; Nakatani, T.; Shiratani, M. Comparison between Ar+CH4 Cathode and Anode Coupling Chemical Vapor Depositions of Hydrogenated Amorphous Carbon Films. *Thin Solid Film.* **2021**, *729*, 138701. [CrossRef]

17. Hwang, S.H.; Okumura, T.; Kamataki, K.; Itagaki, N.; Koga, K.; Shiratani, M. Size and Flux of Carbon Nanoparticles Synthesized by Ar+CH4 Multi-Hollow Plasma Chemical Vapor Deposition. *Diam. Relat. Mater.* **2020**, *109*, 108050. [CrossRef]

18. Jeong, J.I.; Yang, J.H.; Jung, J.H.; Lee, K.H.; Kim, H.J.; Jung, Y.H.; Kim, T.Y.; Lee, M.H.; Hwang, S.H.; Wu, P.; et al. Super Anticorrosion of Aluminized Steel by a Controlled Mg Supply. *Sci. Rep.* **2018**, *8*, 3760. [CrossRef]

19. La, J.; Lee, S.; Hong, S. Surface & Coatings Technology Synthesis of Zn–Mg Coatings Using Unbalanced Magnetron Sputtering and Theirs Corrosion Resistance. *Surf. Coat. Technol.* **2014**, *259*, 56–61. [CrossRef]

20. Park, J.H.; Hagio, T.; Kamimoto, Y.; Ichino, R.; Lee, M.H. Enhancement of Corrosion Resistance by Lamination of Mg Film on Zn-55Al-1.6Si-Coated Steel by Physical Vapor Deposition. *Surf. Coat. Technol.* **2020**, *387*, 125537. [CrossRef]

21. Byun, J.M.; Bang, S.-R.; Kim, H.W.; Kim, T.-Y.; Hong, S.-J.; Kim, Y. Do Effect of Heat Treatment on Corrosion Resistance and Adhesion Property in Zn-Mg-Zn Multi-Layer Coated Steel Prepared by PVD Process. *Surf. Coat. Technol.* **2016**, *309*, 1010–1014. [CrossRef]

22. Ghosh, P.; Mezbahul-Islam, M.; Medraj, M. Critical Assessment and Thermodynamic Modeling of Mg-Zn, Mg-Sn, Sn-Zn and Mg-Sn-Zn Systems. *Calphad Comput. Coupling Phase Diagr. Thermochem.* **2012**, *36*, 28–43. [CrossRef]

23. Ha, H.Y.; Kang, J.Y.; Yang, J.; Yim, C.D.; You, B.S. Role of Sn in Corrosion and Passive Behavior of Extruded Mg-5 Wt%Sn Alloy. *Corros. Sci.* **2016**, *102*, 355–362. [CrossRef]

24. Wang, J.; Li, Y.; Huang, S.; Zhou, X. Study of the Corrosion Behavior and the Corrosion Films Formed on the Surfaces of Mg-XSn Alloys in 3.5 Wt.% NaCl Solution. *Appl. Surf. Sci.* **2014**, *317*, 1143–1150. [CrossRef]

25. Lee, M.H.; Kim, J.D.; Oh, J.S.; Yang, J.H.; Baek, S.M. Morphology and Crystal Orientation on Corrosion Resistance of Mg Thin Films Formed by PVD Method onto Zn Electroplated Substrate. *Surf. Coat. Technol.* **2008**, *202*, 5590–5594. [CrossRef]

26. Jo, Y.H.; Jung, I.; Choi, C.S.; Kim, I.; Lee, H.M. Synthesis and Characterization of Low Temperature Sn Nanoparticles for the Fabrication of Highly Conductive Ink. *Nanotechnology* **2011**, *22*, 225701. [CrossRef]

27. Osório, W.R.; Freire, C.M.; Garcia, A. The Role of Macrostructural Morphology and Grain Size on the Corrosion Resistance of Zn and Al Castings. *Mater. Sci. Eng. A* **2005**, *402*, 22–32. [CrossRef]

28. Dutta, M.; Halder, A.K.; Singh, S.B. Morphology and Properties of Hot Dip Zn-Mg and Zn-Mg-Al Alloy Coatings on Steel Sheet. *Surf. Coat. Technol.* **2010**, *205*, 2578–2584. [CrossRef]

29. Prosek, T.; Persson, D.; Stoulil, J.; Thierry, D. Composition of Corrosion Products Formed on Zn-Mg, Zn-Al and Zn-Al-Mg Coatings in Model Atmospheric Conditions. *Corros. Sci.* **2014**, *86*, 231–238. [CrossRef]

30. Prosek, T.; Nazarov, A.; Goodwin, F.; Šerák, J.; Thierry, D. Improving Corrosion Stability of Zn[Sbnd]Al[Sbnd]Mg by Alloying for Protection of Car Bodies. *Surf. Coat. Technol.* **2016**, *306*, 439–447. [CrossRef]

31. Greer, A.L. Diffusion and Reactions in Thin Films. *Appl. Surf. Sci.* **1995**, *86*, 329–337. [CrossRef]

32. Suzuki, S.; Kakita, K. A Comparative Study of GDOES, SIMS and XPS Depth Profiling of Thin Layers on Metallic Materials. *J. Surf. Anal.* **2005**, *12*, 2–5.

33. Das, S.K.; Kim, Y.M.; Ha, T.K.; Jung, I.H. Investigation of Anisotropic Diffusion Behavior of Zn in Hcp Mg and Interdiffusion Coefficients of Intermediate Phases in the Mg-Zn System. *Calphad Comput. Coupling Phase Diagr. Thermochem.* **2013**, *42*, 51–58. [CrossRef]

34. Yim, C.D.; Yang, J.; Woo, S.K.; Ha, H.Y.; You, B.S. The Effects of Microstructural Factors on the Corrosion Behaviour of Mg-5Sn-XZn (X = 1, 3wt%) Extrusions. *Corros. Sci.* **2015**, *90*, 597–605. [CrossRef]

35. Fu, J.W.; Yang, Y.S. Formation of the Solidified Microstructure in MgSn Binary Alloy. *J. Cryst. Growth* **2011**, *322*, 84–90. [CrossRef]
36. Gualtieri, A.F. Accuracy of XRPD QPA Using the Combined Rietveld-RIR Method. *J. Appl. Crystallogr.* **2000**, *33*, 267–278. [CrossRef]
37. Cao, F.; Shi, Z.; Song, G.L.; Liu, M.; Atrens, A. Corrosion Behaviour in Salt Spray and in 3.5% NaCl Solution Saturated with Mg(OH)2 of as-Cast and Solution Heat-Treated Binary Mg-X Alloys: X = Mn, Sn, Ca, Zn, Al, Zr, Si, Sr. *Corros. Sci.* **2013**, *76*, 60–97. [CrossRef]
38. Yao, C.; Lv, H.; Zhu, T.; Zheng, W.; Yuan, X.; Gao, W. Effect of Mg Content on Microstructure and Corrosion Behavior of Hot Dipped Zn–Al–Mg Coatings. *J. Alloy. Compd.* **2016**, *670*, 239–248. [CrossRef]
39. Salgueiro Azevedo, M.; Allély, C.; Ogle, K.; Volovitch, P. Corrosion Mechanisms of Zn(Mg,Al) Coated Steel: The Effect of HCO3- and NH4+ Ions on the Intrinsic Reactivity of the Coating. *Electrochim. Acta* **2015**, *153*, 159–169. [CrossRef]
40. Volovitch, P.; Vu, T.N.; Allély, C.; Abdel Aal, A.; Ogle, K. Understanding Corrosion via Corrosion Product Characterization: II. Role of Alloying Elements in Improving the Corrosion Resistance of Zn-Al-Mg Coatings on Steel. *Corros. Sci.* **2011**, *53*, 2437–2445. [CrossRef]
41. Kartsonakis, I.A.; Stanciu, S.G.; Matei, A.A.; Hristu, R.; Karantonis, A.; Charitidis, C.A. A Comparative Study of Corrosion Inhibitors on Hot-Dip Galvanized Steel. *Corros. Sci.* **2016**, *112*, 289–307. [CrossRef]
42. Prosek, T.; Nazarov, A.; Bexell, U.; Thierry, D.; Serak, J. Corrosion Mechanism of Model Zinc-Magnesium Alloys in Atmospheric Conditions. *Corros. Sci.* **2008**, *50*, 2216–2231. [CrossRef]
43. Zeng, F.L.; Wei, Z.L.; Li, J.F.; Li, C.X.; Tan, X.; Zhang, Z.; Zheng, Z.Q. Corrosion Mechanism Associated with Mg 2Si and Si Particles in Al-Mg-Si Alloys. *Trans. Nonferrous Met. Soc. China* **2011**, *21*, 2559–2567. [CrossRef]
44. Diler, E.; Lescop, B.; Rioual, S.; Nguyen Vien, G.; Thierry, D.; Rouvellou, B. Initial Formation of Corrosion Products on Pure Zinc and MgZn2 Examined by XPS. *Corros. Sci.* **2014**, *79*, 83–88. [CrossRef]
45. Esmailzadeh, S.; Aliofkhazraei, M.; Sarlak, H. Interpretation of Cyclic Potentiodynamic Polarization Test Results for Study of Corrosion Behavior of Metals: A Review 1. *Prot. Met. Phys. Chem. Surf.* **2018**, *54*, 976–989. [CrossRef]